

This work was written as part of one of the author's official duties as an Employee of the United States Government and is therefore a work of the United States Government. In accordance with 17 U.S.C. 105, no copyright protection is available for such works under U.S. Law.

Public Domain Mark 1.0

<https://creativecommons.org/publicdomain/mark/1.0/>

Access to this work was provided by the University of Maryland, Baltimore County (UMBC) ScholarWorks@UMBC digital repository on the Maryland Shared Open Access (MD-SOAR) platform.

**Please provide feedback**

Please support the ScholarWorks@UMBC repository by emailing [scholarworks-group@umbc.edu](mailto:scholarworks-group@umbc.edu) and telling us what having access to this work means to you and why it's important to you. Thank you.



# Quasi-thermal Noise Spectroscopy Analysis of Parker Solar Probe Data: Improved Electron Density Model for Solar Wind

Oksana Kruparova<sup>1,2</sup> , Vratislav Krupar<sup>1,2</sup> , Adam Szabo<sup>2</sup> , Marc Pulupa<sup>3</sup> , and Stuart D. Bale<sup>3,4</sup>

<sup>1</sup> Goddard Planetary Heliophysics Institute, University of Maryland, Baltimore County, Baltimore, MD 21250, USA; [oksana.kruparova@nasa.gov](mailto:oksana.kruparova@nasa.gov)

<sup>2</sup> Heliospheric Physics Laboratory, Heliophysics Division, NASA Goddard Space Flight Center, Greenbelt, MD 20771, USA

<sup>3</sup> Space Sciences Laboratory, University of California, Berkeley, CA 94720, USA

<sup>4</sup> Physics Department, University of California Berkeley, Berkeley, CA 94720, USA

Received 2023 May 11; revised 2023 August 9; accepted 2023 August 29; published 2023 October 20

## Abstract

We present a comprehensive analysis of electron density measurements in the solar wind using quasi-thermal noise (QTN) spectroscopy applied to data from the first 15 encounters of the Parker Solar Probe mission (2018 November–2023 March). Our methodology involves the identification of the plasma line frequency and the calculation of plasma density based on in situ measurements. By analyzing over 2.1 million data points, we derive a power-law model for electron density as a function of radial distance from the Sun in the range of 13 to 50  $R_{\odot}$ :  $n_e(r) = (343,466 \pm 19921) \times r^{(-1.87 \pm 0.11)}$ . This model provides improved estimates for localizing interplanetary solar radio bursts. Moreover, obtained electron densities can be used for calibrating particle instruments on board the Parker Solar Probe. We discuss its limitations and potential for further refinement with additional Parker Solar Probe encounters.

*Unified Astronomy Thesaurus concepts:* Solar wind (1534); Space plasmas (1544); Radio spectroscopy (1359)

## 1. Introduction

The solar wind is a continuous stream of charged particles emitted from the Sun's outer atmosphere, playing a critical role in shaping the heliosphere and impacting space weather throughout the solar system (Parker 1958). Understanding the characteristics and properties of the solar wind is crucial for advancing our knowledge of the Sun and its effects on space weather, which has implications for satellite operations, communication systems, and even human health during space travel. One of the efficient tools for measuring in situ plasma properties in space is quasi-thermal noise (QTN) spectroscopy, which utilizes a passive wave receiver at the ports of an electric antenna (Meyer-Vernet 1979; Meyer-Vernet et al. 2017).

The Parker Solar Probe mission, launched in 2018, aims to advance our understanding of the solar wind by making in situ measurements closer to the Sun than ever before (Fox et al. 2016). The probe has already completed multiple encounters, providing valuable data that can be analyzed to gain insight into the properties of the solar wind. Moncuquet et al. (2020) presented in situ measurements from the first two encounters of the Parker Solar Probe, revealing different states of the emerging solar wind near the solar activity minimum. These results were obtained from a simplified analysis of the plasma QTN spectrum measured by the Radio Frequency Spectrometer (RFS; FIELDS) described in Bale et al. (2016) and Pulupa et al. (2017).

By analyzing the QTN data collected during the Parker Solar Probe's encounters, one can derive valuable information about the plasma properties, such as electron density, temperatures of the thermal and suprathermal components of the velocity distribution, and the average kinetic temperature. This information can then be used to calibrate particle instruments on board the Parker Solar Probe (Kasper et al. 2016) and

provide a better understanding of the solar wind's behavior near the Sun. The electron density data obtained from QTN analysis also has implications for localizing interplanetary solar radio bursts. Type II and III radio bursts arise from suprathermal electron beams interacting with plasma, generating radio emissions at plasma frequency ( $f_{pe}$ ) or its second harmonic ( $2f_{pe}$ ). As electron beams move away from the Sun, emissions occur at lower frequencies (Wild 1950; Ginzburg & Zhelezniakov 1958). Type II bursts are created by electron beams at shock fronts of coronal mass ejections (CMEs), while type III bursts stem from impulsively accelerated electrons in solar flares.

In this paper, we present an analysis of the QTN data collected during the first 15 encounters of the Parker Solar Probe, focusing on the electron density retrieved from the plasma frequency measurements. The paper is structured as follows: Section 2 describes the data set and methodology used for analyzing the QTN data; Section 3 presents the electron density model derived from the QTN analysis and its comparison with other empirical models; and Section 4 concludes the paper, discussing the implications of the derived model and potential future applications.

## 2. Data and Methodology

This section describes the data set and methodology used to analyze the QTN spectroscopy data obtained from the Parker Solar Probe. The data for this study come from the RFS on board the Parker Solar Probe, which provides in situ measurements of electrostatic fluctuations using signals from the V1–V4 electric field antennas (Bale et al. 2016; Pulupa et al. 2017). We analyze the first 15 encounters of the mission, during which the spacecraft reached down to 13  $R_{\odot}$  from the Sun.

### 2.1. Radio Spectra and Plasma Line Identification

Figures 1(a) and (b) show the radio spectra from the RFS/Low Frequency Receiver (LFR) for 14 days around Encounter



Original content from this work may be used under the terms of the [Creative Commons Attribution 4.0 licence](https://creativecommons.org/licenses/by/4.0/). Any further distribution of this work must maintain attribution to the author(s) and the title of the work, journal citation and DOI.

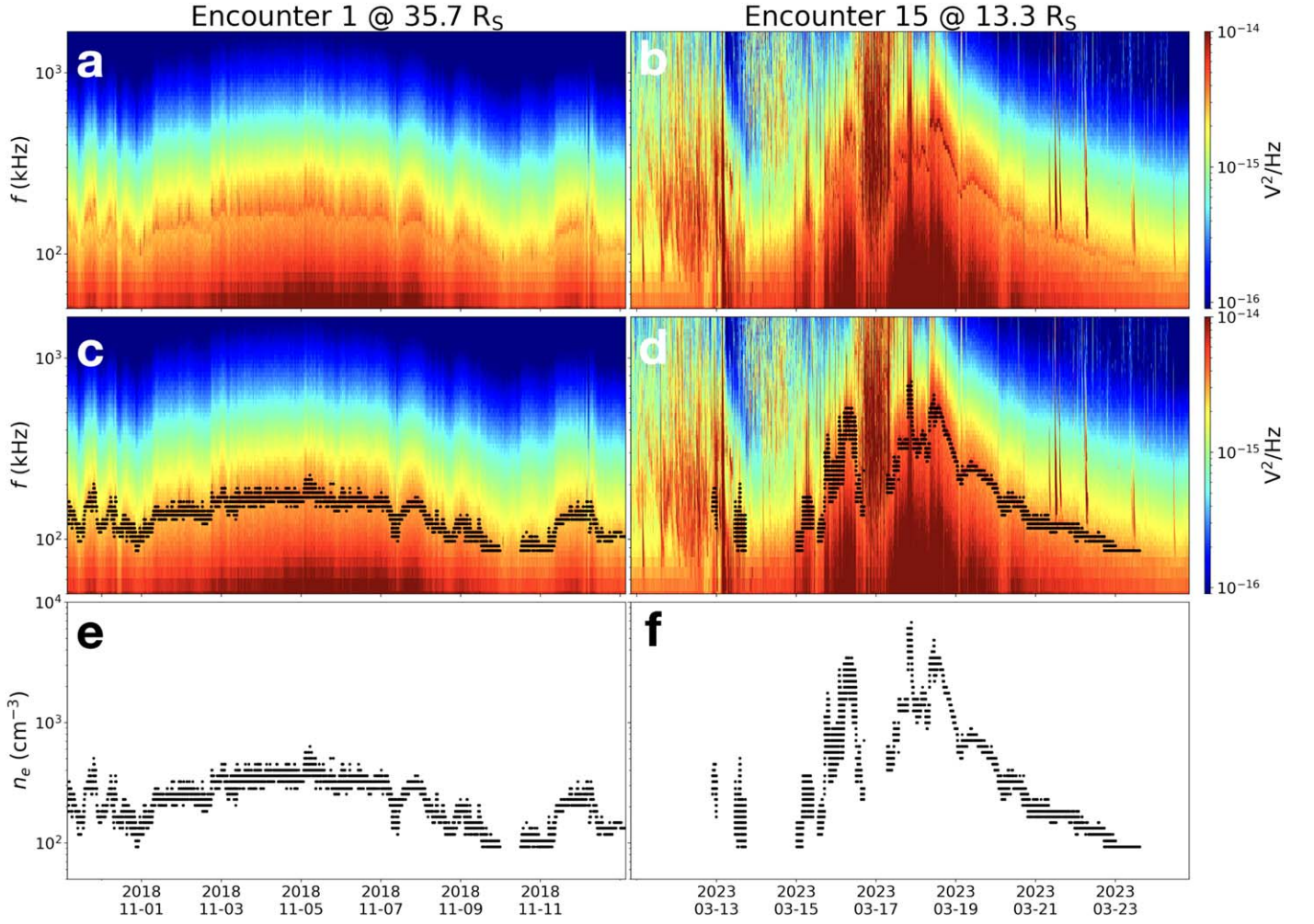


**Figure 1.** (a) and (b) Radio spectra from RFS/LFR for 14 days around Encounter 1 and Encounter 15, respectively. (c) and (d) Obtained plasma frequency  $f_{pe}$  overlapped on the RFS/LFR spectra for Encounter 1 and Encounter 15, respectively. (e) and (f) Obtained electron density  $n_e$  for Encounter 1 and Encounter 15, respectively.

1 and Encounter 15, respectively. During Encounter 1, the plasma line is easily identifiable in the spectra, while in Encounter 15, there are intervals with increased wave activity where the plasma line is not present. To identify the plasma line frequency  $f_L$ , we automatically search for it in a frequency range determined by the density model based on the spacecraft's distance from the Sun. This frequency range is manually adjusted for intervals when the plasma line  $f_L$  occurs at lower or higher frequencies than predicted.

Figure 2 shows an example of our analysis from Encounter 15, where we analyze the voltages detected by the two RFS channels separately (channel 0: V1V2 dipole and channel 1: V3V4 dipole, cross dipole configuration). Figures 2(a) and (b) display the frequency ranges of interest for channel 0 and 1, respectively, denoted by dotted lines. Figures 2(c) and (d) show the same spectra but in a frequency range of our interest and a narrower intensity range. Black circles denote actual data points as measured by the RFS/LFR. We identify local maxima in this frequency interval, and in this case, we obtain a frequency of 514 kHz for both channels. We would like to emphasize that the prior analysis of the first two Parker Solar Probe Encounters conducted by Moncuquet et al. (2020) was confined to the use of a single receiver channel to identify the steepest growth rate near the plasma line, leveraging multiple

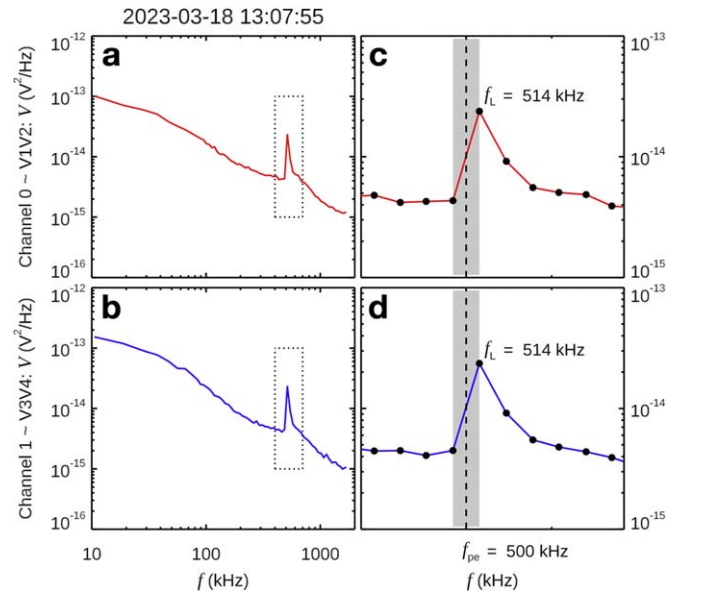


**Figure 2.** Example analysis from Encounter 15. (a) and (b) Frequency ranges denoted by dotted lines for channel 0 and 1, respectively. (c) and (d) Spectra in the frequency range of interest and narrower intensity range with black circles denoting actual data points measured by RFS/LFR.

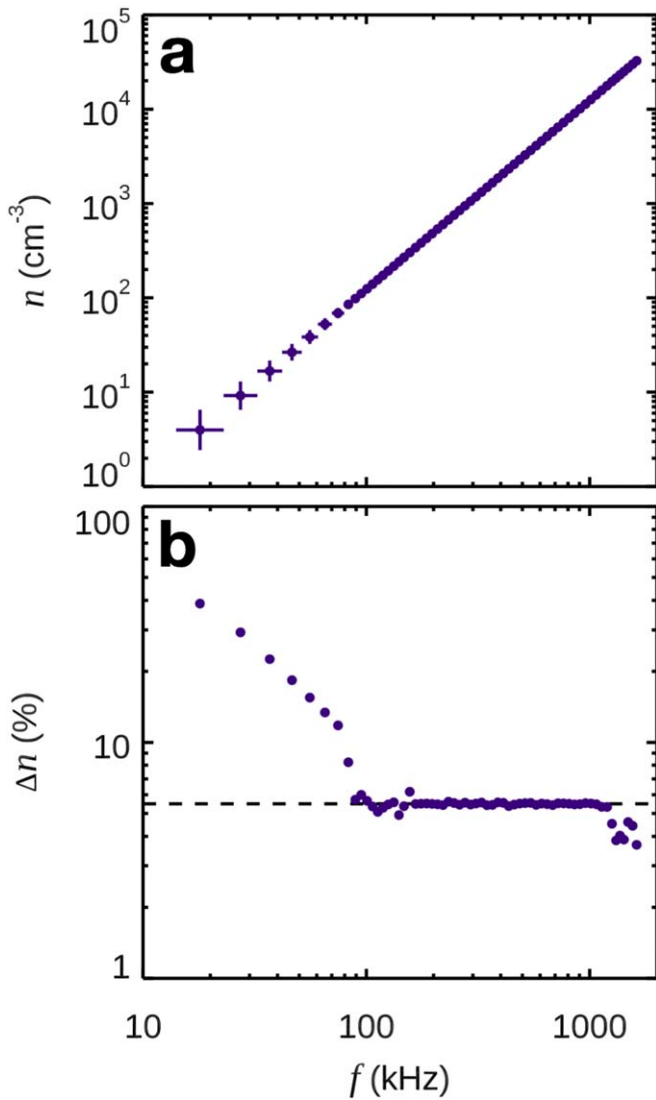


**Figure 3.** (a) Relation between retrieved  $f_{pe}$  and  $n_e$  with error bars intrinsic due to limited frequency resolution of RFS/LFR. (b) Relative error on density as a function of obtained plasma density, demonstrating the suitability of RFS/LFR measurements above 80 kHz or  $80 \text{ cm}^{-3}$ .

frequency channels. Our current work adopts a dual receiver channel approach, differing from the methodology previously employed. We assume that the plasma frequency  $f_{pe}$  is equal to the geometric mean of the plasma line and the preceding frequency channel, which corresponds to the steepest positive slope below the plasma line  $f_L$  (denoted by gray shaded areas in Figures 2(c) and (d)).

The density error bars can be calculated from the frequency resolution of the RFS instrument. Figure 3(a) shows the relation between retrieved  $f_{pe}$  and  $n_e$  with the intrinsic error bars due to the limited frequency resolution of the RFS/LFR. Figure 3(b) shows this error relative to the obtained plasma density, demonstrating that the RFS/LFR provides reasonable measurements only above 80 kHz, or  $80 \text{ cm}^{-3}$ , when the relative error on density is 5.8%. The method is suitable for plasma density measurements closer than  $\sim 100 R_\odot$  from the Sun. However, it is essential to acknowledge that inherent constraints manifest in QTN measurements that fall below the 80 kHz mark. The primary limitation is attributed to the Debye length exceeding the effective antenna lengths of the PSP/RFS

in these low-density conditions. The increase in Debye length in these regions imposes challenges in the accurate assessment of electron densities, thereby demarcating the lower boundary of the method’s effectiveness.

## 2.2. Overview of the Parker Solar Probe Encounters

Figure 4 provides a comprehensive overview of the electron density measurements obtained during the first 15 encounters of the Parker Solar Probe mission, spanning a range of radial distances from the Sun between 13 and  $100 R_\odot$ . Each panel in Figure 4 corresponds to an individual encounter, covering a period of 7 days before and 7 days after the perihelion passage. The data for electron density measurements are depicted by markers with varying colors, wherein the color scale differentiates between groups of encounters based on their respective perihelion distances.

A clear trend of increasing electron density with decreasing radial distance from the Sun is visible in Figure 4, consistent with expectations from solar wind expansion. Data gaps during Encounters 8 and 11, marked by shaded gray areas, are due to data RFS/LFR unavailability. The complete data set, comprising a total of 2,115,146 data points, offers a solid foundation for developing a robust electron density model for the analyzed range of radial distances.

It is worth noting that the Parker Solar Probe mission is still ongoing, and more encounters are expected to be completed in the future. The methodology presented here can be applied to the upcoming data to further improve and extend the electron density model, potentially allowing for a more accurate description of the solar wind environment closer to the Sun, reaching radial distances as small as  $10 R_\odot$ . Additionally, the same approach can be employed to analyze data from other missions, such as the Solar Orbiter (Müller et al. 2020), to better understand the structure and evolution of the solar wind throughout the heliosphere.

## 3. Electron Density Model

In this section, we present the electron density model derived from the QTN data obtained during the first 15 encounters of the Parker Solar Probe (2018 November–2023 March). Furthermore, we compare the proposed model with existing empirical electron density models by Leblanc et al. (1998) and Sittler & Guhathakurta (1999), discussing the relative differences and highlighting the advantages of the new model.

The electron density model is constructed based on 2,115,146 data points collected during the first 15 encounters by Parker Solar Probe. The model employs a power-law function to describe the electron density as a function of radial distance from the Sun. Figure 5 shows a 2D histogram of the obtained electron density versus the radial distance from the Sun. The data points are fitted with the power law:  $n_e(r) = (343,466 \pm 19921) \times r^{(-1.87 \pm 0.11)}$  (solid black line). The error on the retrieved model parameters is assumed to be 5.8% based on the frequency resolution of the RFS/LFR instrument (Figure 3). The corresponding relation for the plasma frequency is  $f_{pe}(r) = (5274 \pm 1270) \times r^{(-0.94 \pm 0.06)}$ . In our analysis, it is essential to underscore certain intrinsic limitations of the method utilized. Specifically, for distances exceeding approximately  $50 R_\odot$ , our electron density data seem to offer a somewhat elevated representation. This is primarily attributed to the method’s predisposition to predominantly



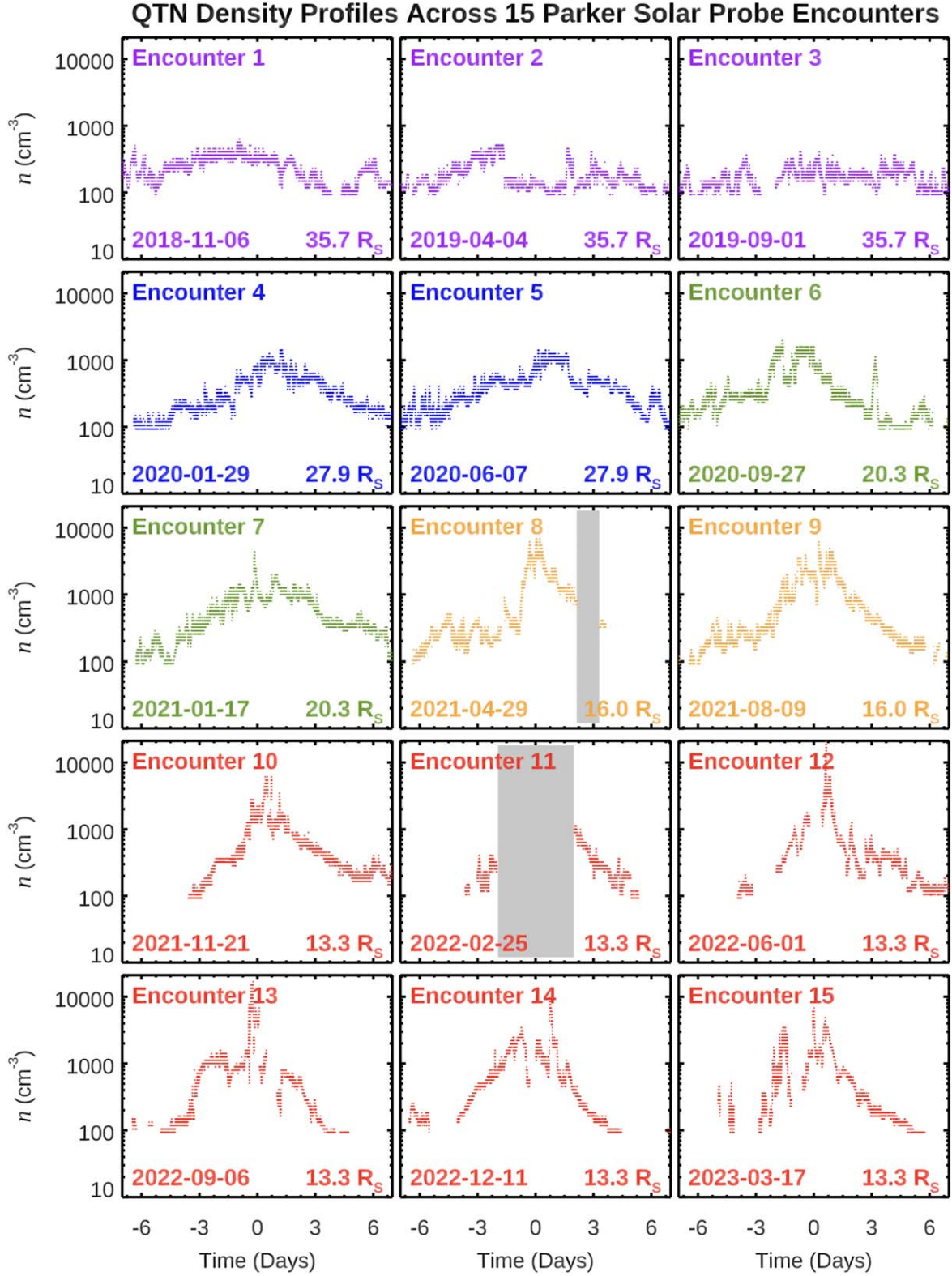


**Figure 4.** Comprehensive display of electron density measurements from the initial 15 encounters of the Parker Solar Probe mission, covering radial distances from the Sun between 13 and 100  $R_{\odot}$ . Each panel pertains to an individual encounter, representing a timeframe of 7 days before and after the closest approach to the Sun (perihelion). The color-coded markers indicate the electron density measurements, with the color scale signifying different encounter groups based on their perihelion distances.

capture  $n_e$  values in excess of  $80 \text{ cm}^{-3}$ . Given this constraint, and to ensure a more accurate portrayal within the bounds of our methodology, we have chosen to circumscribe the applicability of our density model to regions situated below  $50 R_{\odot}$ .

The proposed electron density model is compared with empirical electron density models by Leblanc et al. (1998) and Sittler & Guhathakurta (1999), which are denoted as dashed and dashed-dotted lines, respectively, in Figure 5. It is evident

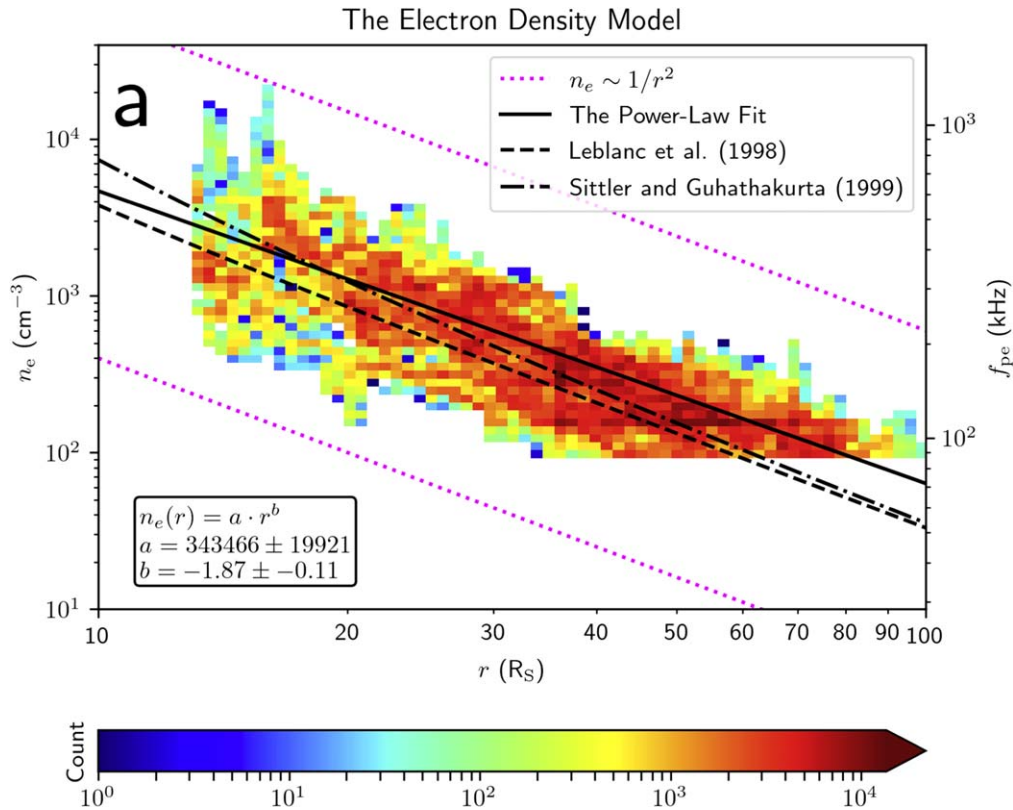


**Figure 5.** A 2D histogram of obtained electron density as a function of radial distance from the Sun based on 2,115,146 data points obtained during the first 15 encounters by Parker Solar Probe. The power-law fit is shown as a solid black line.

that deviations occur for closer and further distances from the Sun between the power-law model and the other two models. While the power-law model is not suitable for predicting electron densities in the corona and near 1 au, it provides accurate estimates for radial distances between 13 and 50  $R_{\odot}$ . The predicted electron density at 1  $R_{\odot}$  is 343,466  $\text{cm}^{-3}$  (i.e., too low), and at 1 au, it is 15  $\text{cm}^{-3}$  (i.e., too high).

A key benefit of the new model is its ability to localize interplanetary solar radio emissions, especially type II and III radio bursts (Dulk 2000). The model offers improved predictions for CME-driven shocks (type II radio bursts; Krupar et al. 2016) and tracking electron beams (type III radio bursts; Krupar et al. 2015). It delivers reliable estimates for radial distances between 13 and 50  $R_{\odot}$ , corresponding to plasma frequency  $f_{pe}$  ranging from 135 to 800 kHz (or 135–800 kHz for fundamental emission and 275–1800 kHz for harmonic emission). In Figure 5, a y-axis for plasma frequency  $f_{pe}$  is also displayed.

Figure 6(a) presents a comparison of the relative differences between our power-law model and the QTN data for radial distances below 50  $R_{\odot}$ . It demonstrates that the power-law model provides the most accurate density estimates for the data obtained during the first 15 encounters of Parker Solar Probe. The power-law model has a mode relative difference of approximately  $-5.81\%$ , indicating a good agreement with the QTN data. The other two models, however, tend to more underestimate the electron density, as shown in Figures 6(b) and (c).

Specifically, the model by Leblanc et al. (1998) underestimates the electron density by 42.77%, resulting in a systematic shift in plasma frequency of 19.49%. Similarly, the model by Sittler & Guhathakurta (1999) underestimates the

electron density by 27.54%, leading to a systematic shift in plasma frequency of 12.93%. These discrepancies highlight the improved precision of our power-law model, which provides more accurate density estimates for radial distances between 13 and 50  $R_{\odot}$ .

It is worth noting that all three models exhibit a long-tail distribution in overestimating the plasma electron density. This can be attributed to periods when Parker Solar Probe is within the fast solar wind, which is characterized by lower plasma density. Nevertheless, the power-law model still outperforms the other two models, providing more reliable density estimates. The simplicity of the power-law model is another advantage over the models by Leblanc et al. (1998) and Sittler & Guhathakurta (1999). Our model only requires two parameters, making it easy to use, while the other models require up to six parameters and more complex equations to cover a wider application range, from the Sun’s surface to 1 au.

#### 4. Conclusions

In this study, we presented an extensive analysis of QTN spectroscopy applied to Parker Solar Probe data, covering the first 15 encounters of the mission (2018 November–2023 March). The QTN data has provided us with valuable in situ measurements of plasma properties in the solar wind, enabling the derivation of a new power-law electron density model for the heliosphere between 13 and 50  $R_{\odot}$ . The data and model presented here have significant implications for understanding and predicting space weather events throughout the solar system, as well as for calibrating particle instruments on board the Parker Solar Probe.

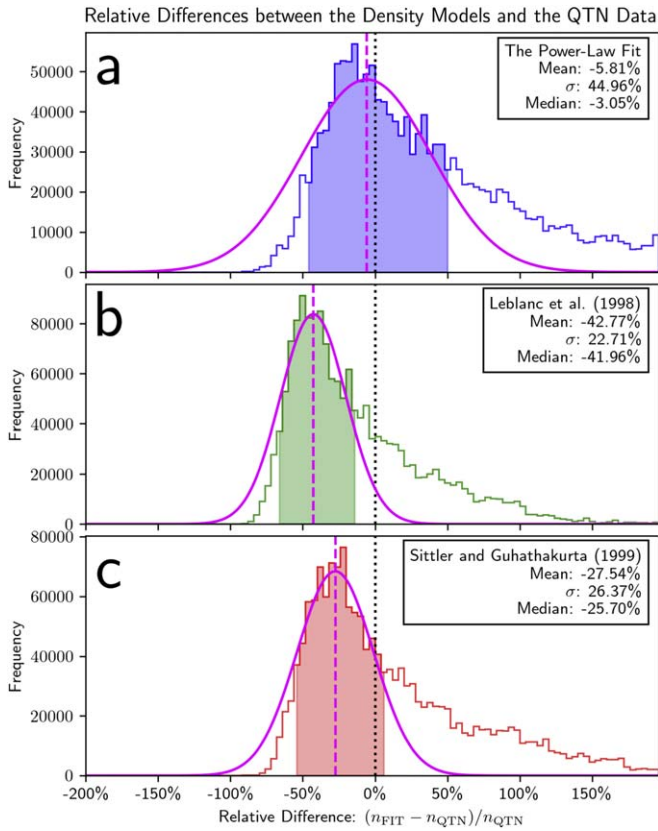


**Figure 6.** Comparison of relative differences between the three density models and the QTN data below  $50 R_{\odot}$ , illustrating the accuracy of the derived power-law model. The shaded regions beneath the histograms signify the FWHM. Magenta lines depict Gaussian fits using data points above the FWHM, with the associated parameters provided in the legend.

Through the analysis of data obtained from RFS on board the Parker Solar Probe, we demonstrated the ability to retrieve accurate measurements of the electron plasma density for a wide range of solar wind conditions (Figures 1–3). The continuous plasma density measurements provide a unique data set that covers a range of distances from the Sun, from the closest approach of  $13 R_{\odot}$  to the furthest at  $100 R_{\odot}$ . This data set, consisting of over 2 million data points, has allowed us to derive a robust power-law electron density model for the heliosphere (Figures 4 and 5). Moreover, it can be used to calibrate particle instruments on board the Parker Solar Probe, further enhancing the scientific return of the mission.

The new power-law electron density model,  $n_e(r) = (343,466 \pm 19921) \times r^{(-1.87 \pm 0.11)}$ , provides an improved description of the electron density distribution in the solar wind compared to previous models (Leblanc et al. 1998; Sittler & Guhathakurta 1999). Notably, our model provides a better fit to the Parker Solar Probe QTN data than the other two models, with an error of only 3.75%. However, it is essential to note that the power-law model is only suitable for radial distances between 13 and  $50 R_{\odot}$ , and should not be applied outside this range.

The availability of accurate electron density measurements and models in the heliosphere is crucial for various applications, including the localization of interplanetary solar radio

bursts, such as type II and III radio bursts, which are essential for understanding energy release and particle acceleration during CMEs and solar flares.

As the Parker Solar Probe mission continues and more data becomes available, we plan to revisit our analysis and refine the electron density model, extending its validity closer to the Sun (up to  $10 R_{\odot}$ ). The methodology presented in this study can also be applied to other missions, such as Solar Orbiter (Müller et al. 2020), further broadening our understanding of the heliosphere and its impact on space weather.

In conclusion, the analysis of QTN spectroscopy applied to Parker Solar Probe data has provided valuable insights into the plasma properties of the solar wind at radial distances between 13 and  $50 R_{\odot}$ . Our derived power-law electron density model offers a simple, yet accurate and reliable tool for estimating electron densities within this radial distance range. This model has important implications for localizing interplanetary solar radio bursts. The QTN data obtained in this study is available to the scientific community via the Space Physics Data Facility (SPDF).<sup>5</sup>

### Acknowledgments

The Parker Solar Probe was designed, built, and is now operated by the Johns Hopkins Applied Physics Laboratory as part of NASA’s Living with a Star (LWS) program (contract NNN06AA01C). Support from the LWS management and technical team has played a critical role in the success of the Parker Solar Probe mission. The FIELDs instrument suite was designed and built and is operated by a consortium of institutions including the University of California, Berkeley, University of Minnesota, University of Colorado, Boulder, NASA/GSFC, CNRS/LPC2E, University of New Hampshire, University of Maryland, UCLA, IFRU, Observatoire de Meudon, Imperial College, London, and Queen Mary University of London.

### ORCID iDs

Oksana Kruparova <https://orcid.org/0000-0002-1122-6422>  
 Vratislav Krupar <https://orcid.org/0000-0001-6185-3945>  
 Adam Szabo <https://orcid.org/0000-0003-3255-9071>  
 Marc Pulupa <https://orcid.org/0000-0002-1573-7457>  
 Stuart D. Bale <https://orcid.org/0000-0002-1989-3596>

### References

- Bale, S. D., Goetz, K., Harvey, P. R., et al. 2016, *SSRv*, 204, 49
- Dulk, G. A. 2000, *GMS*, 119, 115
- Fox, N. J., Velli, M. C., Bale, S. D., et al. 2016, *SSRv*, 204, 7
- Ginzburg, V. L., & Zhelezniakov, V. V. 1958, *SvA*, 2, 653
- Kasper, J. C., Abiad, R., Austin, G., et al. 2016, *SSRv*, 204, 131
- Krupar, V., Eastwood, J. P., Kruparova, O., et al. 2016, *ApJL*, 823, L5
- Krupar, V., Kontar, E. P., Soucek, J., et al. 2015, *A&A*, 580, A137
- Leblanc, Y., Dulk, G. A., & Bougeret, J.-L. 1998, *SoPh*, 183, 165
- Meyer-Vernet, N. 1979, *JGR*, 84, 5373
- Meyer-Vernet, N., Issautier, K., & Moncuquet, M. 2017, *JGRA*, 122, 7925
- Moncuquet, M., Meyer-Vernet, N., Issautier, K., et al. 2020, *ApJS*, 246, 44
- Müller, D., St. Cyr, O. C., Zouganelis, I., et al. 2020, *A&A*, 642, A1
- Parker, E. N. 1958, *ApJ*, 128, 664
- Pulupa, M., Bale, S. D., Bonnell, J. W., et al. 2017, *JGRA*, 122, 2836
- Sittler, E. C., Jr., & Guhathakurta, M. 1999, *ApJ*, 523, 812
- Wild, J. P. 1950, *AuSRA*, 3, 541

<sup>5</sup> [http://spdf.gsfc.nasa.gov/pub/data/psp/fields/13/rfs\\_lfr\\_qtn/](http://spdf.gsfc.nasa.gov/pub/data/psp/fields/13/rfs_lfr_qtn/)